Jansson, P.-E., Kenne, L., Liedgren, H., Lindberg, B., & Lonngren, J. (1976) *Chem. Commun., Univ. Stockholm 8*, 1–75.
Kishimoto, Y., Wajda, M., & Radin, N. S. (1968) *J. Lipid Res. 9*, 27–33.
Klenk, E., & Debuch, H. (1963) *Prog. Chem. Fats Other Lipids 6*, 1–29.
Klenk, E., & Doss, M. (1966) *Hoppe-Seyler's Z. Physiol. Chem. 346*, 296–298.
Klenk, E., & Lohr, J. P. (1967) *Hoppe-Seyler's Z. Physiol. Chem. 348*, 1712–1714.
Klenk, E., Stoffel, W., & Eggers, H. J. (1952) *Hoppe-Seyler's Z. Physiol. Chem. 290*, 246–251.
Kochetkov, N. K., Zhukova, I. G., & Glukhoded, I. S. (1962) *Biochim. Biophys. Acta 60*, 431–432.
Kochetkov, N. K., Zhukova, I. G., & Glukhoded, I. S. (1963) *Biochim. Biophys. Acta 70*, 716–719.
Laine, R. A., Esselman, W. J., & Sweeley, C. C. (1963) *Methods Enzymol. 28*, 159–167.
Larson, G., Karlsson, H., Hansson, G. C., & Pimlott, W. (1987) *Carbohydr. Res. 161*, 281–290.
Leupold, F. (1950) *Hoppe-Seyler's Z. Physiol. Chem. 285*, 182–200.
Levery, S. B., & Hakomori, S. (1987) *Methods Enzymol. 138*, 13–25.
Nimmich, W. (1979) *Z. Allg. Mikrobiol. 19*, 343–347.
Norton, W. T., & Brotz, M. (1963) *Biochem. Biophys. Res. Commun. 12*, 198–203.
Nudelman, E. D., Levery, S. B., Igarashi, Y., & Hakomori, S. (1992) *J. Biol. Chem.* (in press).
Ohashi, Y., Iwamori, M., Ogawa, T., & Nagai, Y. (1987) *Biochemistry 26*, 3990–3995.
Sviridov, A. F., Arifkhodzhaev, K. A., Chizhov, O. S., & Kochetkov, N. K. (1980) *Bioorg. Khim. 6*, 165–186.
Sweeley, C. C., Bentley, R., Makita, M., & Wells, W. W. (1963) *J. Am. Chem. Soc. 85*, 2497–2507.
Tamai, Y. (1968) *Jpn. J. Exp. Med. 38*, 65–73.
Tamai, Y., Taketomi, T., & Yamakawa, T. (1967) *Jpn. J. Exp. Med. 37*, 79–81.
Thierfelder, H., & Klenk, E. (1930) *Die Chemie der Cerebroside und Phosphatide*, p 76, Springer Verlag, Berlin.
Wittenberg, J. B., Korey, S. R., & Swenson, F. H. (1956) *J. Biol. Chem. 219*, 39–47.
Yu, R. K., & Ledeen, R. W. (1972) *J. Lipid Res. 13*, 680–686.

Gramicidin Channels That Have No Tryptophan Residues†

V. Fonseca,‡,§ P. Daumas,‡ L. Ranjalahy-Rasoloarijao,∥ F. Heitz,⊥ R. Lazaro,∥ Y. Trudelle,# and O. S. Andersen*,‡
Department of Physiology and Biophysics, Cornell University Medical College, New York, New York 10021, Laboratoire de Physico-Chimie des Systèmes Polyphasés, CNRS UA330, and Groupe de Recherche Canaux Peptidiques Transmembranaires—Structures et Activités, F-34033 Montpellier, France, Equipe de Recherche Associée au CNRS, UA468, F-34060 Montpellier, France, Centre de Biophysique Moléculaire, CNRS, F-45071 Orleans, France, and Facultad de Fisica, Universidad Complutense, E-28040 Madrid, Spain

Received January 10, 1992; Revised Manuscript Received March 24, 1992

ABSTRACT: In order to understand how aromatic residues modulate the function of membrane-spanning proteins, we examined the role of the four tryptophans in gramicidin A (gA) in determining the average duration and permeability characteristics of membrane-spanning gramicidin channels; the tryptophan residues were replaced by tyrosine (gramicidin T, gT), tyrosine *O*-benzyl ether [gramicidin T(Bzl), gT(Bzl)], naphthylalanine (gramicidin N, gN), and phenylalanine (gramicidin M enantiomer, gM⁻). These analogues form channels with durations and conductances that differ some 10- and 16-fold, respectively. The single-channel conductance was invariably decreased by the Trp → Yyy replacement, and the relative conductance alterations were similar in phosphatidylcholine (DPhPC) and monoglyceride (GMO) bilayers. The duration variations exhibited a more complex pattern, which was quite different in the two membrane environments: in DPhPC bilayers, gN channels have an average duration that is ~2-fold longer than that of gA channels; in GMO bilayers, the average duration of gN channels is about one-tenth that of gA channels. The sequence-dependent alterations in channel function do not result from alterations in the channels' peptide backbone structure, because heterodimers can form between the different analogues and gramicidin A, and there is no energetic cost associated with heterodimer formation [cf. Durkin, J. T., Koeppe, R. E., II, & Andersen, O. S. (1990) *J. Mol. Biol. 211*, 221]. The alterations in permeability properties are consistent with the notion that Trp residues alter the energy profile for ion permeation through long-range electrostatic interactions.

Despite advances in molecular biology and electrophysiology, the molecular mechanisms that underlie ion channel function to remain elusive because only limited structural information is available. General questions concerning channel function can therefore with advantage be examined using appropriate prototypes, such as the channel-forming linear gramicidins. In integral membrane proteins, for example, Trp residues seem to be localized at or near the membrane/solution interface or in the transport path (Chattopadhyay & McNamee, 1991; Henderson et al., 1990; Michel & Deisenhofer, 1990). But the structural or functional significance of this arrangement remains obscure.

† This work was supported by NIH Grant GM21342 and by NSF Grant NSF-INT-8413704.
* To whom correspondence should be addressed.
‡ Cornell University Medical College.
§ Universidad Complutense.
∥ Equipe de Recherche Associée au CNRS.
⊥ CNRS UA330 and G. d. R. Canaux Peptidiques Transmembranaires.
Centre de Biophysique Moléculaire, CNRS.

0006-2960/92/0431-5340$03.00/0

The naturally occurring linear gramicidins are hydrophobic pentadecapeptides (Sarges & Witkop, 1965; Gross & Witkop, 1965), HCO-L-Xxx[1]-Gly[2]-L-Ala[3]-D-Leu[4]-L-Ala[5]-D-Val[6]-L-Val[7]-D-Val[8]-L-Trp[9]-D-Leu[10]-L-Yyy[11]-D-Leu[12]-L-Trp[13]-D-Leu[14]-L-Trp[15]-NH-CH_2CH_2-OH, where Xxx can be either Val or Ile while Yyy is Trp, Phe, or Tyr (in gramicidins A, B, or C, respectively). The alternating L–D sequence permits gramicidins to form helical structures in which the polar peptide groups line a central pore, while the nonpolar side chains project from the exterior surface [Urry, 1971; Veatch et al., 1974; see Andersen et al. (1992) for a recent review]. Membrane-spanning gramicidin channels form by the transmembrane association of two right-handed $\beta^{6.3}$-helices, at their formyl–NH termini, in an antiparallel arrangement (Arsen'ev et al., 1985; Nicholson & Cross, 1989; O'Connell et al., 1990; Koeppe et al., 1992). The site of dimerization is at the center of the symmetrical channel, which is stabilized by six intermolecular (peptide) hydrogen bonds. The four Trp's in each monomer are thus close to the membrane/solution interface, which makes gA (and its analogues) suitable to examine general questions pertaining to the structural and functional importance of Trp residues (Becker et al., 1991).

The magnitude of the single-channel conductance is determined primarily by the polar backbone, but the conductance varies when the amino acid sequence of the channel formers is altered (Bamberg et al., 1976; Morrow et al., 1979; Heitz et al., 1982; Prasad et al., 1983; Mazet et al., 1984; Durkin et al., 1986, 1990; Russell et al., 1986; Koeppe et al., 1990, 1992; Sawyer et al., 1990; Becker et al., 1991; Daumas et al., 1991). These conductance changes could result from changes in channel structure, from side-chain-dependent modulations in the energy profile for ion movement through the channels, or from a combination of these effects. Experiments on channels formed by gramicidins with a series of ring-substituted phenylalanines at position 1, at the channel's center, show that a dominant mechanism underlying the conductance changes involves through-space ion–dipole interactions (Koeppe et al., 1990).

Conductance changes are also induced by amino acid replacements in the COOH-terminal half of the molecule, which is close to the channel entrance at the membrane/solution interface. The naturally occurring Trp → Phe substitution in gB, for example, induces an almost 2-fold decrease in the single-channel conductance (Bamberg et al., 1976; Sawyer et al., 1990). When all four Trp's in gA were replaced by Phe, the resulting gM^- (M enantiomer) form channels with a single-channel conductance that (in 1.0 M CsCl) is 15–20-fold less than that of gA (or gA^-) channels (Heitz et al., 1982; Koeppe et al., 1992).

To address the question of how the aromatic residues in gramicidin channels determine the channel permeability and duration, we synthesized gramicidin analogues in which all four Trp residues in gramicidin A (gA) were replaced by the following residues (Figure 1): Tyr in gramicidin T (gT), *O*-benzyl-Tyr in gramicidin T(Bzl) [gT(Bzl)], naphthylalanine in gramicidin N (gN), and Phe in the enantiomeric gramicidin M^- (gM^-). In this paper, we address the question, whether the channels formed by gA and these analogues are structurally equivalent, and characterize the basic functional alterations induced by the modifications.

Some of these results have appeared in preliminary form (Fonseca et al., 1989).

Experimental Approach

The structure of bilayer-incorporated gramicidin channels has not been solved by direct methods, which poses problems

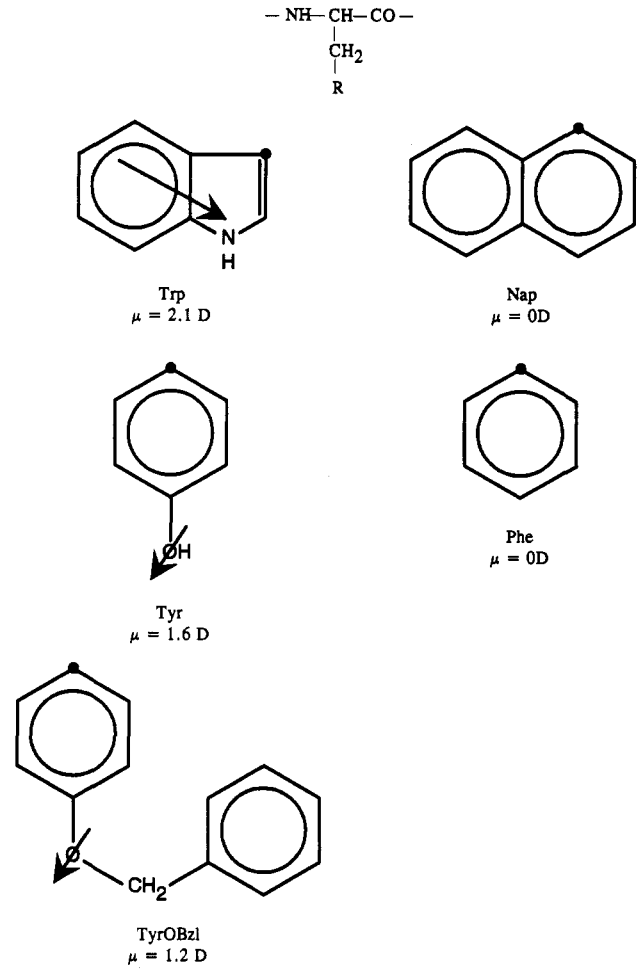

FIGURE 1: Chemical modifications at positions 9, 11, 13, and 15. At the top are illustrated the peptide backbone and the β-methylene group. Below are the different aromatic rings that were used. The rings are identified by their associated amino acid. The rings are attached to the β-methylene at ●. The dipole moments are from Smyth (1955) [the moment for Tyr(Bzl) is estimated from that of Tyr-O-CH_3]. The arrows denote the approximate orientations of the dipole moment vectors of the rings (Smyth, 1955; Weiler & Feilchenfeld, 1970).

for attempts to relate the structure of channels formed by sequence-modified gramicidins to the gA channel structure. It is possible to circumvent this problem, however, by addressing the related question: are the channels formed by the modified gramicidins structurally *equivalent* to the reference channel [cf. Durkin et al. (1990)]? This question can be examined using a functional approach because conducting gramicidin channels are symmetrical dimers in equilibrium with nonconducting, membrane-adsorbed monomers (Bamberg & Läuger, 1973; Veatch et al., 1975; Cifu et al., 1992) and channels formed by the linear gramicidins have a single predominant conducting state (Andersen et al., 1987; Busath et al., 1987; Sawyer et al., 1989). Channels formed by a given gramicidin therefore can be associated with a given single-channel behavior (average conductance and duration). If two gramicidins with different sequences (e.g., A and B) form homodimeric channels (A–A and B–B) that have equivalent peptide backbone structures, asymmetrical heterodimers (A–B and B–A) should form between the chemically dissimilar gramicidins. These heterodimers can be detected in single-channel experiments as new channel types: the hybrid channels. The energy profile for ion movement through the channel may be different for the two orientations; this asymmetry will be discernible as a difference in the current through the A → B and B → A channels (Apell et al., 1977; Mazet et al., 1984;

Russell et al., 1986; Sawyer et al., 1990; Becker et al., 1991; Cifu et al., 1992; Koeppe et al., 1992; see Results).

That hybrid channels form shows that the formyl–NH termini in the dissimilar ($\beta^{6.3}$-helical) monomers can adapt to each other when forming the heterodimer, but the backbone structure in each homodimer could still differ. To test for this possibility, we measured the heterodimer appearance rates (f_{hl} and f_{hh}, respectively, for the low- and high-conductance hybrid channels) relative to the appearance rates for the two (parent) homodimers (f_a and f_b), as well as the average durations of the heterodimers (τ_{hl} and τ_{hh}) relative to those of the homodimers (τ_a and τ_b). The activation energy for forming heterodimers relative to that for forming homodimers ($\Delta\Delta G^{\ddagger}$) is given by (Durkin et al., 1992)

$$\Delta\Delta G^{\ddagger} = -(RT/2) \ln \{f_{hl}f_{hh}/(f_a f_b)\} \quad (1)$$

where R and T denote the gas constant and temperature in kelvin, respectively, and $\Delta\Delta G^{\ddagger}$ is determined relative to the arithmetic mean of the $\Delta G^{\ddagger}$'s for the two symmetrical channel types (Durkin et al., 1990). The standard free energy difference of the heterodimers relative to the homodimers ($\Delta\Delta G^{\circ}$) is correspondingly given by (Durkin et al., 1992)

$$\Delta\Delta G^{\circ} = -(RT/2) \ln \{[\tau_{hl}\tau_{hh}/(\tau_a\tau_b)][f_{hl}f_{hh}/(f_a f_b)]\} \quad (2)$$

where $\Delta\Delta G^{\circ}$ again is determined relative to the arithmetic mean of the ΔG°'s for the two symmetrical channel types. [If the two heterodimer orientations are indistinguishable, i.e., if there is only a single hybrid channel type, eqs 1 and 2 reduce to those employed by Durkin et al. (1990).] If $\Delta\Delta G^{\ddagger} \simeq 0$, the two homodimeric channels are structurally equivalent, an argument that is strengthened when also $\Delta\Delta G^{\circ} \leq 0$, in which case there is no strain on the join between the monomers in the heterodimer [see Durkin et al. (1990) for further discussion].

Materials and Methods

HPLC-purified gA was a gift from Dr. R. E. Koeppe II (University of Arkansas). gT was synthesized as described by Trudelle and Heitz (1987). In order to avoid secondary reactions during the synthesis, the tyrosine –OH groups were protected by benzyl groups (Bzl), which were later removed. gT(Bzl) is thus an intermediate in the synthesis of gT. gN was synthesized as described by Ranjalahy-Rasoloarijao et al. (1989) and gM^- as described by Heitz et al. (1982). For the bilayer experiments, the gramicidins were dissolved in absolute ethanol (U.S. Industrial Chemicals, Toscula, IL).

Diphytanoylphosphatidylcholine (DPhPC) was from Avanti Polar Lipids (Pine Bluffs, AL). It gave a single spot on thin-layer chromatograms and was further cleaned by ion-exchange chromatography (Andersen, 1983). *n*-Decane was 99.9% pure from Wiley Organics (Columbus, OH) and was used without further purification. Glycerol monooleate (GMO) was from Sigma Chemical Co. (St. Louis, MO). CsCl was Ultrapure grade from United States Biochemicals (Cleveland, OH). Before use it was roasted at 550 °C for at least 24 h and stored over NaOH in evacuated desiccators. All other chemicals were reagent grade. The water was deionized Millipore Milli-Q water (Millipore Corp., Bedford, MA).

Experimental Procedures. Planar lipid bilayers were formed from DPhPC dissolved in *n*-decane at 25 ± 1 °C by the pipet technique of Szabo et al. (1969) across a hole (1.4 or 0.3 mm in diameter) in a Teflon partition separating two Teflon chambers, each containing 5 mL of 1.0 M CsCl (pH ≃ 6). (A limited set of experiments were done in GMO/*n*-decane). The gramicidins were added to give a single-channel activity of ~1 channel appearance/s. The necessary gramicidin concentration differed for each analogue and was determined empirically. For gA, the final nominal concentration was ~10 pM; for gN, it was ~1 nM.

For most experiments, aliquots of the appropriate gramicidin, or of the appropriate mixture of gramicidins, were added symmetrically to both aqueous phases. In some experiments, the orientations of the two hybrid channels were determined by adding the gramicidins asymmetrically: a different gramicidin was added to each electrolyte solution after a stable bilayer had been formed.

Single-channel measurements were made using the bilayer punch (Andersen, 1983) using a home-built current-to-voltage converter. Contact to the aqueous solutions was through Ag/AgCl electrodes. The membrane potential difference (V) is measured relative to the rear (or trans) solution.

The amplitude of single-channel current transitions and the times of channel appearance and disappearance events were measured on-line using the algorithm described by Andersen (1983). Current transition amplitude histograms and channel duration histograms were generated off-line [cf. Durkin et al. (1990)].

For each channel type (and potential) the reported single-channel currents [$i(V)$] are based on at least 500 transitions from at least four measurements, two at each polarity. In the case of symmetrical channels, the results at different polarities were simply averaged; in the case of asymmetrical channels, the results for the high- and low-conductance channel types were averaged separately. The results are given as mean ± standard deviation on the basis of a weighted average of the results from the individual measurements, using the number of channels as the weight function.

For each channel type, identified by its characteristic conductance, the appearance rate (f) was determined from the number of current transitions (n) in the appropriate peak in the amplitude histogram [$f = n/(2T_{obs})$, where T_{obs} denotes the duration of the experiment]. At each potential, the average single-channel durations ($\tau(V)$) were determined by matching channel appearances and disappearances and measuring the elapsed time. If two, or more, channels of the same type were conducting simultaneously, a random number generator was used to associate channel appearances with disappearances. The resulting table of channel durations was used to construct survivor plots [e.g., Andersen and Muller (1982)]. Estimates for the average channel duration (τ) were obtained by fitting a single exponential decay, $N(t) = N(0) \exp\{-t/\tau\}$, where t is time, $N(t)$ the number of events with a duration longer than t, and $N(0)$ the estimated number of events in the population, to the results using a maximum-likelihood estimator (Hall & Sellinger, 1981).

Results

Experiments with Single Gramicidin Analogues: Symmetrical Channels. Each gramicidin analogue forms conducting channels that have a characteristic conductance. This is illustrated in Figure 2, which shows current traces for gA, gT, gT(Bzl), gN, and gM^- channels, respectively, in GMO and DPhPC membranes. Both the single-channel current amplitudes and the average durations vary with the nature of the aromatic side chains and bilayer composition. The currents in GMO membranes are about 2-fold higher than in DPhPC membranes, irrespective of the type of aromatic side chain (see also Table I). The alterations in channel duration are more subtle. For gA and gT channels, τ is not significantly affected by the changes in membrane lipid composition; for gT(Bzl),

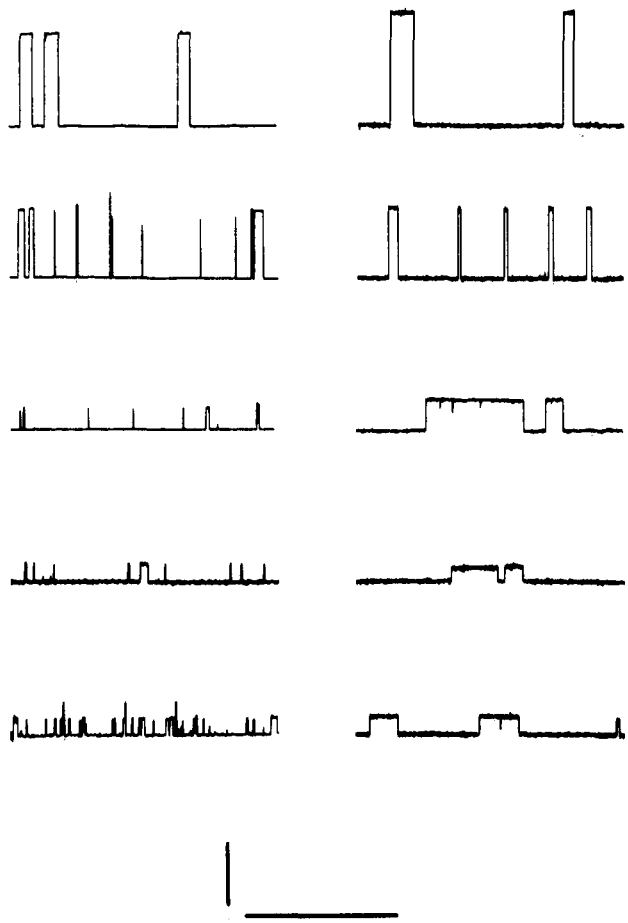

FIGURE 2: Single-channel transitions observed in GMO (left) and DPhPC (right) bilayers. From top to bottom, the channels are formed by gA, gT, gT(Bzl), gN, and gM^-. The vertical calibration bars denote 10 pA (left) and 5 pA (right). The horizontal calibration bars denote 5 s.

Table I: Single-Channel Currents and Durations in DPhPC and GMO Membranes

	DPhPC		GMO	
analogue	$i(200)$ (pA)	$\tau(200)$ (ms)	$i(200)$ (pA)	$\tau(200)$ (ms)
gA	9.7 ± 0.2	570	16.7 ± 0.1	540
gT	6.4 ± 0.1	80	12.5 ± 0.1	130
gT(Bzl)	2.6 ± 0.1	730	4.7 ± 0.1	70
gN	1.3 ± 0.1	1000	3.0 ± 0.2	60
gM^-	1.6 ± 0.1	330	3.0 ± 0.2	50

gM^-, and gN channels, τ is 5–10-fold larger in DPhPC than in GMO membranes (Table I).

The variations in the single-channel currents [$i(V)$] with the type of aromatic residue are further illustrated in Figure 3, which shows current transition amplitude histograms obtained in DPhPC membranes. In all cases single and narrow peaks were observed, indicating that each analogue forms channels that have a single predominant conducting state. At this potential (200 mV), the magnitude of the single-channel current transitions varies 7-fold between gA and gN channels.

The aromatic side-chain-dependent variations in τ are quantified in survivor histograms (Figure 4). For each channel type, the survivor plots are well described by a single exponential decay—again indicating that each analogue forms a single predominant channel type. At this potential (200 mV), there is a 10-fold variation in channel duration between gT and gN channels. The quantitative variation in τ is similar to that observed for $i(200)$, but there is no clear correlation between τ and $i(200)$.

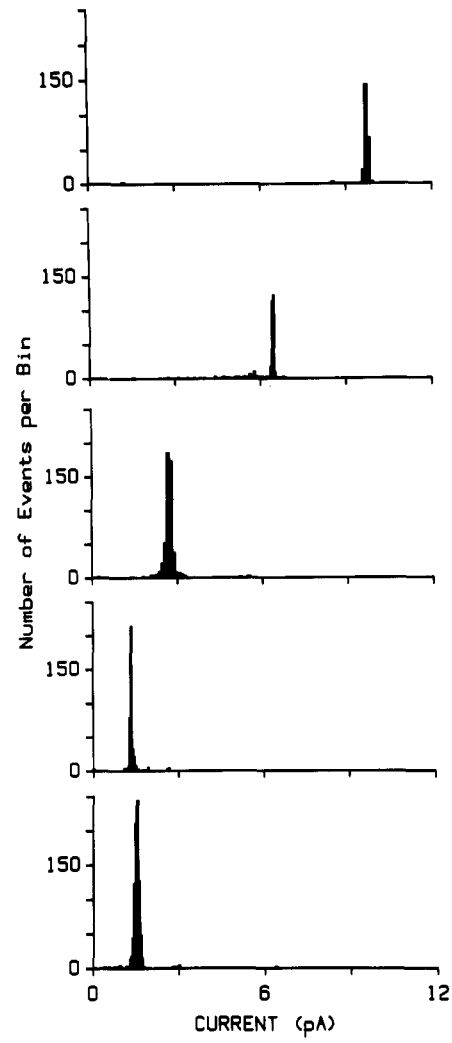

FIGURE 3: Current transition amplitude histograms in DPhPC membranes. From top to bottom, channels formed by gA, gT, gT(Bzl), gN, and gM^-. The average currents are summarized in Table I: 200 mV.

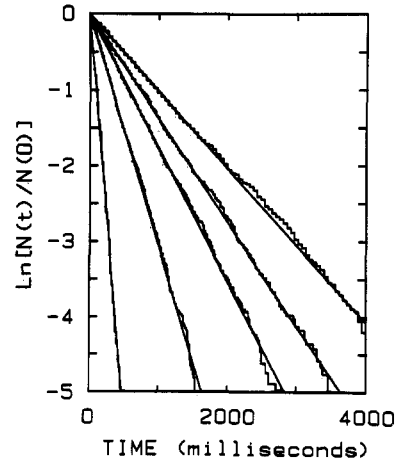

FIGURE 4: Duration distributions in DPhPC membranes. The results are presented as normalized survivor plots. From left to right, channels formed by gT, gM^-, gA, gT(Bzl), and gN. The durations are summarized in Table I: 200 mV.

The voltage dependence of the single-channel conductances and durations varies with the type of aromatic residue in the homodimers (Table II and Figure 5). Table II summarizes information on the average small-signal conductance (g, determined at ±25 and 50 mV) and duration (τ, determined at ±25, 50, 75, and 100 mV). Figure 5 shows the normalized

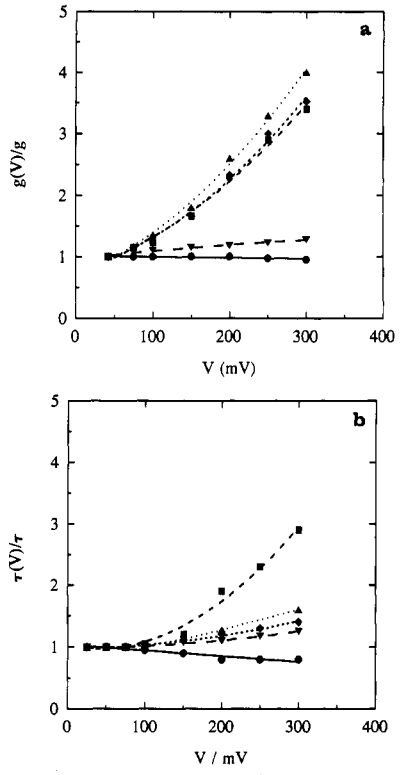

FIGURE 5: Voltage dependence of the single-channel conductances and average durations. The symbols denote (●) gA, (▼) gT, (■) gT(Bzl), (◆) gN, and (▲) gM⁻. Panels: (a) normalized conductances, $g(V)/g$; (b) normalized durations, $\tau(V)/\tau$. g and τ are from Table II.

Table II: Small-Signal Conductances and Durations in DPhPC Membranes[a]

analogue	g (pS)	τ (ms)
gA	49.3 ± 1.5	760
gT	25.7 ± 1.1	60
gT(Bzl)	6.6 ± 0.1	340
gN	3.0 ± 0.2	750
gM⁻	3.6 ± 0.2	160

[a] The small-signal conductance (g) is based on measurements at ±25 and ±50 mV. The average duration (τ) is based on measurements ±25, ±50, ±75, and ±100 mV.

conductance and duration variations as a function of V.

The small-signal conductances vary 16-fold, with gA and gN channels being the extreme cases (Table II). This variation in g is associated with a large variation in the voltage dependence of the conductance (Figure 5a). For (the high-conductance) gA and gT channels, the single-channel conductance is approximately voltage-independent (25 mV $\leq V \leq$ 300 mV); for (the low-conductance) gT(Bzl), gN, and gM⁻ channels the conductance at 300 mV is 3–4-fold larger than the small-signal conductance g.

The small-signal durations vary 10-fold, with the extremes being gT and gN channels. Below 100 mV, τ is essentially voltage-independent. At higher potentials, the average duration increases as a function of V, except for gA channels (Figure 5b). There is no clear correlation between the side-chains' chemical structure and the voltage-dependent changes in average duration (see Discussion).

Experiments with Two Gramicidin Analogues: Asymmetrical Channels. The large variations in permeability characteristics and average duration that are induced by replacing the four Trp's in gA by other aromatic residues could result because the amino acid replacements induced significant changes in the structure of channels formed by the different gramicidins. In order to examine if this were the case, we tested whether conducting heterodimers, or hybrid channels, can form between the different gramicidins.

An experiment of this kind is illustrated in Figure 6, which shows results obtained with gA and gT(Bzl). When either compound was added alone, to both sides of the membrane, only a single-channel type is observed (top and middle current traces and amplitude histograms). When both compounds were added to both sides of the membrane (lower trace and amplitude histogram), one observes the same two (homodimeric) channel types as were seen in the upper traces as well as two new channel types with intermediate current transition amplitudes. These new channel types are seen only when both gramicidins are added to both aqueous phases; they are therefore heterodimers, or hybrid channels.

Also with gN and gT, hybrid channels form when gA and one of the analogues are added to both sides of a bilayer. The hybrid channels are represented by the central two peaks in the amplitude histograms, while the symmetrical channels correspond to the outermost two peaks—the one representing gA channels at the larger current amplitude (Figure 7). No hybrid channels were observed between gM⁻ and gA [or between gM⁻ and gT(Bzl) in GMO membranes], because gM⁻ forms channel with a helix sense that is opposite to that of channels formed by the other gramicidins used in this study, such that the hydrogen-bonded join cannot form (Koeppe et al., 1992).

The two heterodimer orientations were identified in experiments where the gramicidins were added asymmetrically to preformed bilayers (Figure 8). (For technical reasons, these experiments were done using membranes with an diameter of 0.3 mm, which provides access to the solutions on both sides of the bilayer but also decreases the signal-to-noise ratio compared to the other experiments.) gA was added to the trans solution, which is the electrical reference, while the analogue, gN, was added to the cis solution. Depending on the polarity of the applied potential (±200 mV), two different channel types were observed and two different amplitude histograms were obtained (Figure 8, top and middle). At each polarity, there was a single predominant peak in the histogram. The high-conductance channel type was observed when the gA half of the heterodimer was positive, i.e., when the net flux was due to ions entering the heterodimer at the gA end; the low-conductance channel type was observed when the gN half of the heterodimer was positive, when the net ion flow was in the opposite direction.

At the end of the experiment, the membrane was broken, a new membrane was formed after 30–60 s (the delay allowed some gramicidin to mix between the two solutions), and a new current amplitude histogram was obtained (Figure 8, bottom). The two channel types that were observed at asymmetrical conditions correspond to the two heterodimer types in the "symmetrical" experiment (cf. Figures 6 and 7).

Similar results were obtained with gA + gT(Bzl) (results not shown). Again, the high-conductance heterodimer was the one in which the gA half was toward the positive solution.

The normalized conductance–voltage relations for the different heterodimer combinations are shown in Figure 9. For each analogue pair, both the low- and the high-conductance hybrid channels have conductances that are intermediate to those of the two corresponding symmetrical channels. For the gA + gT mixture, the conductances of the two hybrid channel types are essentially voltage-independent [the orientation of these channels was not determined directly but inferred from the results with gA + gT(Bzl) and gA + gN]. For the gA

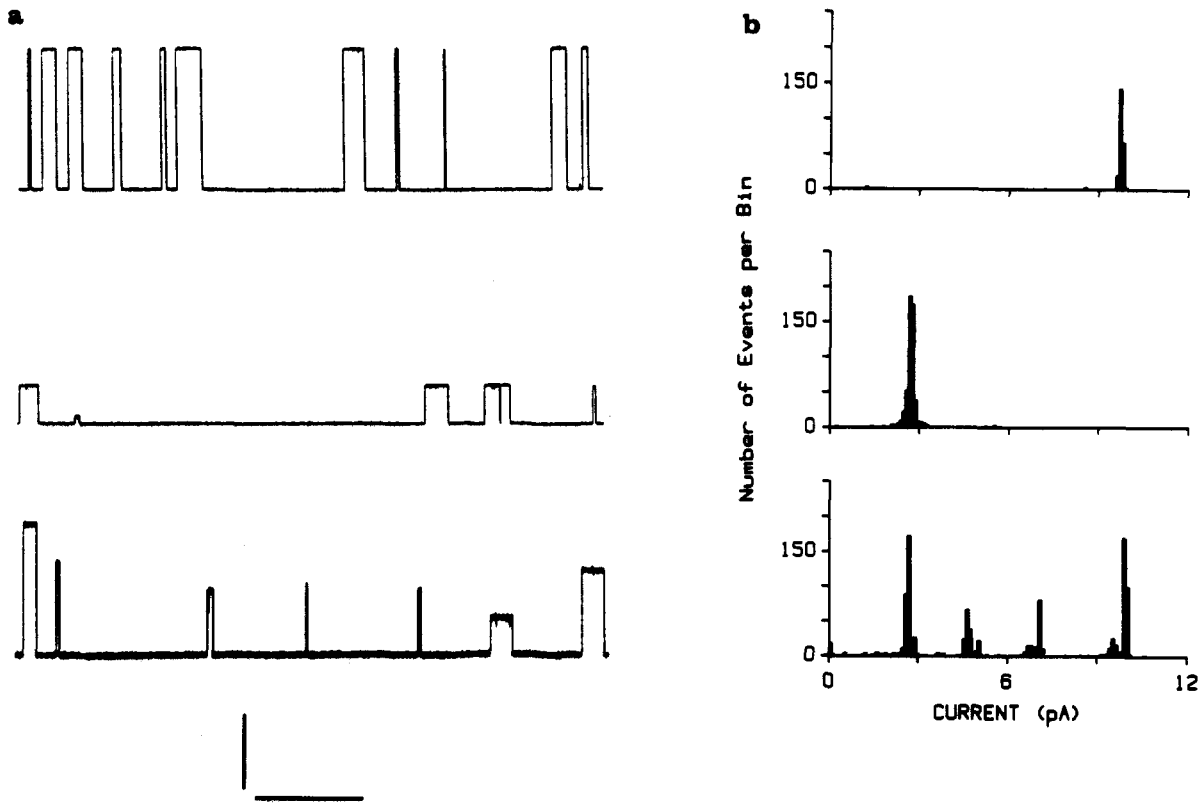

FIGURE 6: Hybrid channel experiment: heterodimers form between gA and gT(Bzl). (a) Single-channel current traces observed with gA (top), gT(Bzl) (middle), and their mixture (bottom). Both symmetrical channel types as well as two new channel types, the hybrid channels, appear in the lower trace. The calibration bars denote 5 pA (vertically) and 5 s (horizontally). (b) Current transition amplitude histograms obtained with only gA (top), gT(Bzl) (middle), and with their mixture (bottom). The top histogram contains 247 transitions, of which 234 (or 95%) are in the peak at 9.7 pA. The middle histogram contains 1060 transitions: 319 (30%) in the peak at 2.6 pA; 128 (12%) in the peak at 4.6 pA; 103 (10%) in the peak at 7.0 pA; and 276 (26%) in the peak at 9.8 pA. The middle two peaks correspond to the hybrid channels: 200 mV.

+ gN and the gA + gT(Bzl) mixtures, the hybrid channel types have conductances that are approximately linear functions of V, but with different slopes for the two heterodimer orientations. The high-conductance orientations [gA → gN and gA → gT(Bzl)] have the steeper voltage dependence—which again is steeper for gA + gN than for gA + gT(Bzl). Because of the different voltage dependencies of the high- and low-conductance heterodimers, the relative "split" between the high- and low-conductance orientation (defined as $2[g_{hh} - g_{hl}]/[g_{hh} + g_{hl}]$ will vary as a function of V. At 300 mV, the relative split was 0.1 for gA + gT, 0.3 for gA + gT(Bzl), and 0.6 for gA + gN.

The average durations of the different heterodimers were determined from the channel duration distributions. Figure 10 depicts normalized survivor plots for the two heterodimer orientations observed with gA + gN. Similar results were observed with gA + gT and gA + gT(Bzl) (not shown). For all channel types, the results are well described by single exponential decays—again indicating that each hybrid channel type (in the amplitude histograms) indeed corresponds to a single, unique dimer type [cf. Cifu et al. (1992)].

For each combination, the two hybrid channel orientations have quite different average durations (with the high-conductance hybrid channel type being the most stable). For the gA + gT mixture, the two hybrid channel types have approximately voltage-independent average durations, which is intermediate to those of the two symmetrical channel types. For the other combinations [gA + gT(Bzl) and gA + gN], both heterodimer orientations have average durations that vary as a function of V (Figure 11). For these combinations, the average durations of the heterodimers were, at low potentials, less than those of either of the corresponding symmetrical channel types. With increasing V, the average durations of the high-conductance (gA → gX) hybrid channel types increased severalfold—much more than those of the low-conductance (gX → gA) hybrid channel types. [At 300 mV, the average durations of both the gA → gN and the gA → gT(Bzl) heterodimers are *longer* than those of either of the corresponding homodimers.]

Table III: Heterodimer Durations and Relative Appearance Rate

analogue pair	τ_{hl} (ms)	τ_{hh} (ms)	$(f_{hl}f_{hh}/(n_a n_b))^{0.5}$
gT/gA	240	230	1.3 ± 0.4
gT(Bzl)/gA	320	450	0.7 ± 0.3
gN/gA	290	810	2.9 ± 0.7
gM^-/gA^- [a]	320	470	2.6 ± 0.6

[a] From Koeppe et al. (1992). 200 mV.

Table IV: Relative Free Energies of Heterodimer Formation and Stability

analogue pair	$\Delta\Delta G^{\ddagger}$ (kJ/mol)	$\Delta\Delta G^{\circ}$ (kJ/mol)
gT/gA	−0.7	−1.0
gT(Bzl)/gA	0.9	2.2
gN/gA	−2.6	−1.5
gM^-/gA^- [a]	−2.4	−1.9

[a] From Koeppe et al. (1992). 200 mV.

The results on single-channel appearance rates and average durations are summarized in Table III. [gM^- cannot form heterodimers with gA, but it does do so with the enantiomer gA^- (Koeppe et al., 1992); the results from these experiments are also summarized in Tables III and IV.] From this in-

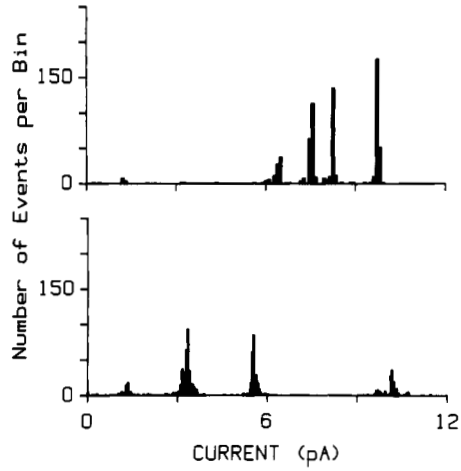

FIGURE 7: Current transition amplitude histograms obtained with symmetrical addition of gA + gT (top) and gA + gN (bottom): 200 mV.

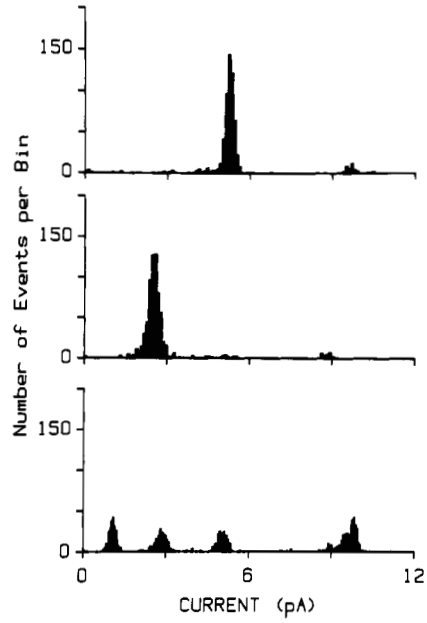

FIGURE 8: Hybrid channel experiment: orientation of gA + gN heterodimers. The analogues were added asymmetrically, one to each side of a preformed bilayer. Current transition amplitude histograms were obtained when the gA-containing solution was positive (top) and when it was negative (bottom). Channels lasting longer than 100 ms were used to determine the current transition amplitudes. The top histogram contains 613 transitions, of which 505 (or 82%) are in the hybrid channel peak at 5.2 pA. The middle histogram contains 572 transitions, of which 422 (or 74%) are in the main peak at 2.6 pA. The bottom histogram (obtained after the membrane was broken and re-formed) contains 2340 transitions: 472 (20%) in the gN peak at 1.1 pA; 408 (17%) in the hybrid peak at 2.8 pA; 402 (17%) in the hybrid peak at 5.0 pA; and 704 (30%) in the gA peak at 9.6 pA (200 mV).

formation we can calculate the $\Delta\Delta G^{\ddagger}$, the activation energy for hybrid channel formation (relative to the two symmetrical channel types), as well as the standard free energy for the hybrid channels (again relative to the symmetrical channels) using eqs 1 and 2. The results are summarized in Table IV.

For all combinations tested here, $\Delta\Delta G^{\ddagger} \leq RT/2$ (at 25 °C, RT = 2.5 kJ/mol), indicating that there is no significant energetic cost associated with hybrid channel formation (the formation of gN + gA and gA^{-} + gM^{-} heterodimers is favored). $\Delta\Delta G^{\ddagger}$ is within RT of zero, usually favoring the heterodimers. gT(Bzl) is an exception, as both $\Delta\Delta G^{\ddagger}$ and $\Delta\Delta G^{\circ}$ are positive. Caution is necessary when using this

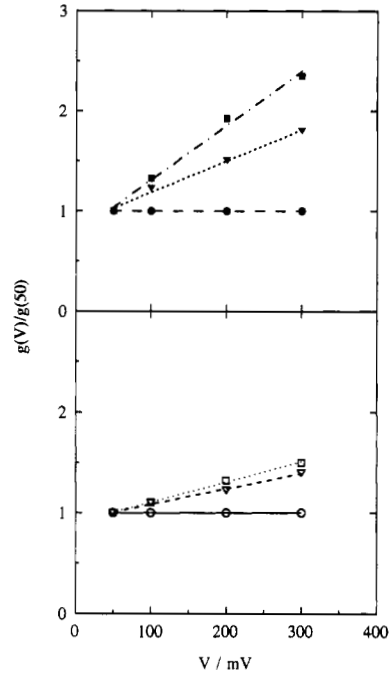

FIGURE 9: Normalized conductance–voltage relations for the hybrid channels, $g(V)/g(50)$, as a function of V for heterodimers formed by gA + gT, gA + gT(Bzl), and gA + gN. The top panel shows results for the high-conductance hybrid channels (the gA → gX direction). The symbols denote (●) gA → gT, (▼) gA → gT(Bzl), and (■) gA → gN. The bottom panel shows results for the low-conductance hybrid channels (the gX → gA direction). The symbols denote (○) gT → gA, (▽) gT(Bzl) → gA, and (□) gN → gA. The straight lines have no theoretical significance.

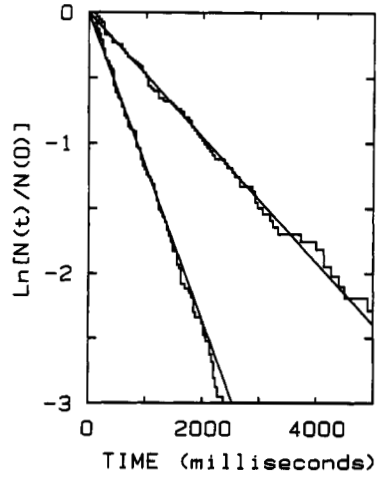

FIGURE 10: Normalized heterodimer duration distributions for heterodimers formed by gA + gN. For gA → gN, τ = 2200 ms; for gA → gA, τ = 760 ms (300 mV).

analogue to study the functional role of Trp.

Discussion

Gramicidin analogues in which all four Trp's are replaced by other aromatic residues form channels that have features similar to those of gA channels (channel appearances and disappearances being simple rectangular current transitions). Nevertheless, the permeability characteristics (and the average duration) of the different channel types differ by more than 1 order of magnitude. The changes in permeability characteristics occur even though the side chains do not interact directly with the permeating ions, which raises the two questions. Are the analogue channels structurally equivalent to gA channels? If affirmative, what are the mechanisms by

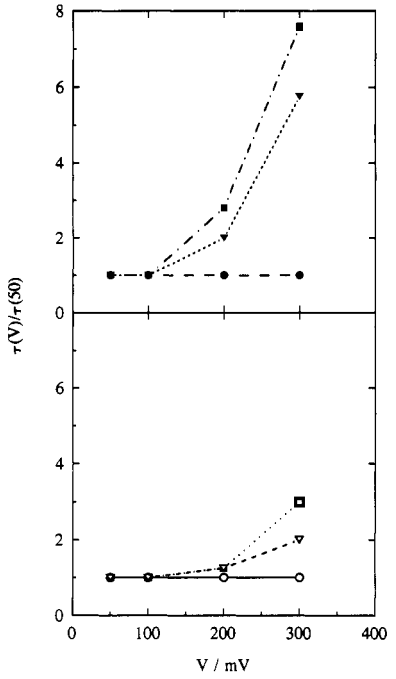

FIGURE 11: Normalized duration–voltage relations for the hybrid channels, $\tau(V)/\tau(50)$, as a function of V for heterodimers formed by gA + gT, gA + gT(Bzl), and gA + gN. The top panel shows results for the high-conductance hybrid channels (the gA → gX direction). The symbols denote (●) gA → gT, (▼) gA → gT(Bzl), and (■) gA → gN. The bottom panel shows results for the low-conductance hybrid channels (the gX → gA direction). The symbols denote (○) gT → gA, (▽) gT(Bzl) → gA, and (□) gN → gA. The curves have no theoretical significance.

which the side-chain replacement can alter the channels' behavior?

We first address the question of structural equivalence among the analogue channels. Then we address the altered permeability characteristics and the alterations in channel duration. Finally, we briefly discuss some implications of these results.

Structural Equivalence among Sequence-Substituted Gramicidin Channels? When only a single gramicidin type was added to both sides of a bilayer, each analogue formed only a single predominant channel type (Figures 2–4): in current transition amplitude histograms (Figure 3), the channels formed by each analogue define a single characteristic peak, which shows that the analogues are chemically homogeneous; and the duration distributions for the channels in the major peak in the amplitude histograms can be described by simple exponential decays (Figure 4). Together, these findings indicate that each of these gramicidin analogues forms channels with a single predominant peptide backbone structure (and molecularity).

The question remains, whether the amino acid substitutions alter the channel (peptide backbone) structure. That does not appear to be the case. First, hybrid channels form between the various analogues; the peptide backbone structures are thus identical or able to adapt to each other when forming the membrane-spanning channels. Second, the activation energy for hybrid channel formation relative to symmetrical channel formation ($\Delta\Delta G^{\ddagger}$, Table IV) was $\leq RT/2$ (RT = 2.5 kJ/mol at 25 °C), which indicates that the different analogues need not refold (or readjust) in order to form hybrid channels as compared to the symmetrical channels. This argues that gramicidin analogues with a wide variety of Trp → Phe substitutions form channels whose peptide backbone is structurally equivalent to that of gA channels [cf. Becker et al. (1991)]. [$\Delta\Delta G^{\ddagger}$ is negative, by about $-RT$, for the $gA^- + gM^-$ and gA + gN heterodimers. That is, heterodimer formation is *favored* relative to the formation of the symmetrical parent channels. We tentatively ascribe this behavior to differences in the way in which the completely apolar phenylalanine or naphthylalanine residues and the amphipathic tryptophan, tyrosine, or tyrosine *O*-benzyl ether residues can be accommodated in the membrane and/or interact with the membrane/solution interface [cf. Becker et al. (1991)].] Third, the standard free energy of the hybrid channels relative to the symmetrical channels was similar to $\Delta\Delta G^{\ddagger}$ for gA + gT and gA + gM (actually $gA^- + gM^-$), which indicates that there was no strain on the join between the monomers. [In the case of gA + gN and gA + gT(Bzl) heterodimers $\Delta\Delta G^{\circ}$ was $\sim RT/2$ positive to $\Delta\Delta G^{\ddagger}$, and there could be a strain on the join between gN or gT(Bzl) and gA. In order to evaluate this question further, one will need analogues with 1–3 substitutions [cf. Becker et al. (1991)]. In any case, caution should be exerted when these analogues are used to examine the functional role of the Trp residues.]

The energetics of heterodimer formation, however, is primarily a test for peptide backbone strain at the join between the monomers and gross structural alterations, such as a change in helix sense. Our results do not exclude that the side-chain substitutions induce some (minor) strain or structural alteration of the backbone near the channel entrance, at the membrane/solution interface.

We finally note that we never observe more than two hybrid channel types and that each identifiable hybrid channel type appears to be molecularly homogeneous (each hybrid channel peak in the current transition amplitude histograms has duration distributions that can be described by single exponential decays; cf. Figure 11). These findings provide strong additional support for the notion that gramicidin channels are *dimers* rather than some higher oligomers as has been proposed (Stark et al., 1986); see Cifu et al. (1992) and Andersen and Koeppe (1992) for further discussion. [Additionally, Daumas (1988) found that the voltage- or temperature-induced conductance relaxation in bilayers modified by the Trp- → Yyy-substituted gramicidin analogues used here did not differ significantly from those obtained in gA-modified membranes, which indicates that lateral association cannot be of importance for channel formation. Indeed, when a 31 amino acid gramicidin is used (retrogramicidin A–D-Ala–gramicidin A; Lelievre et al., 1989), which can span the membrane as a monomer, there were no detectable conductance relaxations.]

Permeability Characteristics. Ion movement through gramicidin channels can, to a first approximation, be described by the following sequence of steps [cf. Andersen and Procopio (1980)]: diffusion from one bulk solution to the channel entrance; association with the channel, which involves a (stepwise) ion dehydration and resolvation by the carbonyl oxygens in the pore wall; translocation through the pore; dissociation, which involves the (stepwise) desolvation and rehydration; and diffusion from the entrance into the other bulk solution.

The order in which the substitutions alter the conductance is the same in DPhPC and GMO membranes (Table I), and the relative conductance changes are almost invariant between these host bilayers. For a given analogue, the ~2-fold different conductances in DPhPC and GMO are presumably a consequence of the interfacial dipole potential being ~120 mV more positive in monoglyceride as compared to phospholipid membranes (Hladky & Haydon, 1973), which will be reflected in the energy barrier for ion movement through the channel

interior (Jordan, 1983). That the relative conductance changes are comparable in these different membrane environments suggests further that the side-chain substitutions alter the conductance by altering ion channel interactions directly rather than by altering the way in which the channels are accommodated by the membrane.

The sequence modifications are at the channel entrances, and one might conclude that the conductance alterations arise from changes in the rate constants for ion entry and exit. By itself, however, that does not account for the correlation between a decreased small-signal conductance and an increased voltage dependence of the single-channel conductance (Table I and Figure 5a). The increased voltage dependence should vary as a function of the *ratio* of the dissociation and translocation rate constants [e.g., Andersen (1989)]—the higher the ratio, the steeper the voltage dependence. The present results [and those of Daumas et al. (1989, 1991)] thus suggest that the translocation rate constant is decreased as well; see also Heitz et al. (1989). [This conclusion would hold unconditionally if the channels were occupied by at most one ion; but gA channels can be occupied by two Cs^+ (Finkelstein & Andersen, 1981), which complicates the analysis. Detailed kinetic analysis of ion movement through channels formed by gA analogues with single Trp → Phe substitutions confirms, however, that both the entry/exit and the translocation rate constants are altered by the substitution and that a Trp → Phe substitution at either of positions 9, 11, 13, and 15 decreases the translocation rate constant with varying effects on the entry/exit rate constants (Becker et al., 1992; M. D. Becker, R. E. Koeppe II, and O. S. Andersen, manuscript in preparation).]

In any case, the conductance changes cannot be ascribed to just the presence of dipolar residues at positions 9, 11, 13, and 15 because even though Tyr and Tyr(Bzl) have comparable dipole moments, gT and gT(Bzl) form channels whose small-signal conductances differ ~5-fold. It thus appears that the *orientation* of the dipolar residues must be important [cf. Becker et al. (1991) and Daumas et al. (1991)], which implies that the side chains must have rather static orientations (in the sense that the permeating ions do not significantly affect the side-chain orientations). Similarly, experiments with gramicidins that had quinoline substitutes at the β-carbon (at positions 9, 11, 13, and 15) showed that the conductance could vary ~10-fold as the dipole orientation in the ring was altered (Daumas, 1988). The average orientations of the amphipathic Trp and Tyr residues are most likely determined by hydrogen-bonded connections between the NH and OH moieties and polar groups at the membrane/solution interface, such that the dipole moments ar directed toward the aqueous solution [cf. Becker et al. (1991)]. If the much more bulky Tyr(Bzl) residues also were hydrogen-bonded to the membrane/solution interface, the average dipole moment would be directed toward the membrane interior, such that Tyr and Tyr(Bzl) would be nonequivalent in terms of their effects on channel function.

The suggestion that Trp → Yyy substitutions near the channel entrances decrease the rate constant for translocation through the channel is consistent with the electrostatic calculations of Sancho and Martinez (1991), which show that a ring of axial dipoles near the entrance can alter the electrostatic potential energy at the channel's center. If the indole group's dipole moment is directed toward the membrane/solution interface (see above), the Trp's will produce a negative electrostatic potential at the channel center—which will serve to increase the translocation rate constant [cf. Becker et al. (1991) and Sancho and Martinez (1991)].

That Trp → Yyy substitutions can induce large changes in the channels' catalytic efficiency (single-channel conductance) is also evident by the presence of two clearly identifiable hybrid channel types, which correspond to the two hybrid channel orientations (Figures 8 and 9). The two orientations can be distinguished because the amino acids in the two monomers have different contributions to the energy profile for the permeating ions, such that the overall energy barrier is asymmetrical. In the presence of an applied potential difference, the currents through the gA → gX and gX → gA orientations of the heterodimers will thus differ.

At a given potential, the current is larger in the gA → gX direction than in the gX → gA direction. This indicates that the major energy barrier is in the gX half of the heterodimer, which could arise from an increase in the barrier for ion entry per se; from an asymmetry in the barrier for traversing the channel, with a maximum in the gX half of the channel; or from a combination of these factors. An alteration (increase) in the barrier for ion entry could arise because ion entry is associated with a (partial) dehydration, in which all but two of the H_2O molecules surrounding an incoming ion are replaced by carbonyl oxygens from the pore wall. Ion solvation by the backbone will alter the backbone geometry, which could alter the side-chain position relative to the membrane/solution interface [cf. Urry (1973)]. If ion coordination is associated with an outward movement of the aromatic residues, a replacement of the amphipathic Trp or Tyr residues by less polar (or nonpolar) residues could result in an increased barrier for entry because of the increased energetic cost associated with the channel's (side-chain) response to ion entry.

An alteration (increase) of the energy barrier deeper into the gX half of the heterodimer could result because the Trp dipoles in gA establish a negative electrostatic potential in the gA half of the channel (Sancho & Martinez, 1991), which would serve to counteract a preexisting image potential (Levitt, 1978; Jordan, 1984) and thus produce a relative decrease in the energy barrier for ion movement.

Channel Duration. Trp → Phe substitutions alter not only the single-channel conductance but also the channels' average duration (τ). In contrast to the conductance changes, however, there is no clear pattern in the duration changes. Indeed, the most striking aspect of these results is that the pattern of variations in τ is different in DPhPC and GMO membranes (Table I). That τ varies as a function of the membrane environment as well as the identity of the amino acid residues at positions 9, 11, 13, and 15 suggests that the duration is a function of how the side chains interact with the membrane/solution interface, either because the side chains alter the energetics of deforming the membrane [Sawyer et al., 1989; Becker et al., 1991; see also Huang (1986)] or because subtle changes in side-chain position (and backbone structure) are transmitted to the join.

At this time, the voltage dependence of the hybrid channel durations (Figure 11) is also an enigma, because it is the high-conductance hybrid channels that have the longer durations. This result excludes the "obvious" explanation: an effect of the applied potential on the side-chain dipoles, where the interaction energy would be of different sign for the two heterodimer orientations. The Trp dipoles in the gA half of the high-conductance hybrid channels point toward the (positive) aqueous solution and should have an unfavorable interaction with the field. On the basis of a simple electrostatic model, one would thus expect that the high-conductance hybrid channels should have the shorter average duration.

Conclusions. The aromatic residues at positions 9, 11, 13, and 15 in the linear gramicidins are important determinants of gramicidin channel function. The channel durations (and relative channel stability) vary as the Trp side chains are replaced by other residues, but in a manner that depends on the composition of the host bilayer. The results suggest that the amphipathic character (hydrogen-bonding ability) of the residues is important in terms of orienting the side chains, which may also account for the orientation of Trp residues in the photosynthetic reaction center (Michel & Deisenhofer, 1990). The small-signal conductance changes are consistent with the notion that side-chain dipoles alter the electrostatic potential at the channel center—some 1–1.5 nm from where the sequence substitutions were made—and that the conductance changes primarily arise from alterations of long-range ion–dipole interactions (Mazet et al., 1984; Etchebest & Pullman, 1988; Koeppe et al., 1990). Interfacial Trp residues in other membrane proteins, e.g., the photosynthetic reaction center (Michel & Deisenhofer, 1990) and bacteriorhodopsin (Henderson et al., 1990), may similarly affect function through long-range electrostatic interactions.

Acknowledgments

We thank M. D. Becker, R. E. Koeppe II, G. Martinez, and M. Sancho for helpful discussions.

References

Andersen, O. S. (1983) *Biophys. J. 41*, 119–133.
Andersen, O. S. (1989) *Methods Enzymol. 171*, 62–112.
Andersen, O. S., & Muller, R. U. (1982) *J. Gen. Physiol. 80*, 403–426.
Andersen, O. S., & Koeppe, R. E., II (1992) *Biophys. J. 61*, 590.
Andersen, O. S., Koeppe, R. E., II, Durkin, J. T., et al. (1987) in *Ion Transport Through Membranes* (Yagi, K., & Pullman, B., Eds.) pp 295–314, Academic Press, Tokyo.
Andersen, O. S., Sawyer, D. B., & Koeppe, R. E., II (1992) in *Biomembrane Structure and Function* (Gaber, B. P., & Easwaran, K. R. K., Eds.) pp 227–244, Adenine Press, Schenectady, NY.
Apell, H.-J., Bamberg, E., Alpes, H., et al. (1977) *J. Membr. Biol. 31*, 171–188.
Arsen'ev, A. S., Barsukov, I. L., Bystrov, V. F., et al. (1985) *FEBS Lett. 186*, 168–174.
Bamberg, E., & Läuger, P. (1973) *J. Membr. Biol. 11*, 177–194.
Bamberg, E., Noda, K., Gross, E., et al. (1976) *Biochim. Biophys. Acta 419*, 223–228.
Becker, M. D., Greathouse, D. V., Koeppe, R. E., II, et al. (1991) *Biochemistry 30*, 8830–8839.
Becker, M. D., Koeppe, R. E., II, & Andersen, O. S. (1992) *Biophys. J.* (in press).
Busath, D. D., Andersen, O. S., & Koeppe, R. E., II (1987) *Biophys. J. 51*, 79–88.
Chattopadhyay, A., & McNamee, M. G. (1991) *Biochemistry 30*, 7159–7164.
Cifu, A. S., Koeppe, R. E., II, & Andersen, O. S. (1992) *Biophys. J. 61*, 189–203.
Daumas, P. (1988) Gramicidines Lineaires: Contribution a L'Etude de la Relation Structure Chimique-Activite Ionagogue, Thesis, Academie de Montpellier.
Daumas, P., Heitz, F., Ranjalahy-Rasoloarijao, L., et al. (1989) *Biochimie 71*, 77–81.
Daumas, P., Benamar, D., Heitz, F., et al. (1991) *Int. J. Pept. Protein Res. 38*, 218–228.
Durkin, J. T., Andersen, O. S., Blout, E. R., et al. (1986) *Biophys. J. 49*, 118–121.
Durkin, J. T., Koeppe, R. E., II, & Andersen, O. S. (1990) *J. Mol. Biol. 211*, 221–234.
Durkin, J. T., Koeppe, R. E., II, & Andersen, O. S. (1992) *J. Mol. Biol.* (submitted for publication).
Etchebest, C., & Pullman, A. (1988) *Jerusalem Symp. Quantum Chem. Biochem. 21*, 167–185.
Finkelstein, A., & Andersen, O. S. (1981) *J. Membr. Biol. 59*, 155–171.
Fonseca, V., Daumas, P., Ranjalahy-Rasoloarijao, L., et al. (1989) *Biophys. J. 55*, 502a.
Gross, E., & Witkop, B. (1965) *Biochemistry 4*, 2495–2501.
Hall, P., & Sellinger, B. (1981) *J. Phys. Chem. 85*, 2941–2946.
Heitz, F., Spach, G., & Trudelle, Y. (1982) *Biophys. J. 40*, 87–89.
Heitz, F., Van Mau, N., Bennes, R., et al. (1989) *Biochimie 71*, 83–88.
Henderson, R., Baldwin, J. M., Ceska, T. A., et al. (1990) *J. Mol. Biol. 213*, 899–929.
Hladky, S. B., & Haydon, D. A. (1973) *Biochim. Biophys. Acta 318*, 464–468.
Huang, H. W. (1986) *Biophys. J. 50*, 1061–1070.
Jordan, P. C. (1983) *Biophys. J. 41*, 189–195.
Jordan, P. C. (1984) *J. Membr. Biol. 78*, 91–102.
Koeppe, R. E., II, Mazet, J.-L., & Andersen, O. S. (1990) *Biochemistry 29*, 512–520.
Koeppe, R. E., II, Providence, L. L., Greathouse, D. V., et al. (1992) *Proteins 12*, 49–62.
Lelievre, D., Trudelle, Y., Heitz, F., et al. (1989) *Int. J. Pept. Protein Res. 33*, 379–385.
Levitt, D. G. (1978) *Biophys. J. 22*, 209–219.
Mazet, J. L., Andersen, O. S., & Koeppe, R. E., II (1984) *Biophys. J. 45*, 263–276.
Michel, H., & Deisenhofer, J. (1990) *Curr. Top. Membr. Transp. 36*, 53–69.
Morrow, J. S., Veatch, W. R., & Stryer, L. (1979) *J. Mol. Biol. 132*, 733–738.
Nicholson, L. K., & Cross, T. A. (1989) *Biochemistry 28*, 9379–9385.
O'Connell, A. M., Koeppe, R. E., II, & Andersen, O. S. (1990) *Science 250*, 1256–1259.
Prasad, K. U., Trapane, T. L., Busath, D., et al. (1983) *Int. J. Pept. Protein Res. 22*, 341–349.
Ranjalahy-Rasoloarijao, L., Lazoro, R., Daumas, P., et al. (1989) *Int. J. Pept. Protein Res. 33*, 273–280.
Russell, E. W. B., Weiss, L. B., Navetta, F. I., et al. (1986) *Biophys. J. 49*, 673–686.
Sancho, M., & Martinez, G. (1991) *Biophys. J. 60*, 81–88.
Sarges, R., & Witkop, B. (1965) *J. Am. Chem. Soc. 87*, 2011–2019.
Sawyer, D. B., Koeppe, R. E., II, & Andersen, O. S. (1989) *Biochemistry 28*, 6571–6583.
Sawyer, D. B., Williams, L. P., Whaley, W. L., et al. (1990) *Biophys. J. 58*, 1207–1212.
Smyth, C. P. (1955) *Dielectric Behavior and Structure*, McGraw-Hill Book Co., New York.
Stark, G., Strässle, M., & Takacz, Z. (1986) *J. Membr. Biol. 89*, 23–37.
Szabo, G., Eisenman, G., & Ciani, S. (1969) *J. Membr. Biol. 1*, 346–382.
Trudelle, Y., & Heitz, F. (1987) *Int. J. Pept. Protein Res. 30*, 163–169.
Urry, D. W. (1971) *Proc. Natl. Acad. Sci. U.S.A. 68*, 672–67.

Urry, D. W. (1973) *Jerusalem Symp. Quantum Chem. Biochem. 5*, 723-736.
Veatch, W. R., Fossel, E. T., & Blout, E. R. (1974) *Biochemistry 13*, 5249-5256.
Veatch, W. R., Mathies, R., Eisenberg, M., et al. (1975) *J. Mol. Biol. 99*, 75-92.
Weiler-Feilchenfeld, H., Pullman, A., Berthod, H., et al. (1970) *J. Mol. Struct. 6*, 297-304.

Aggregation of IgE-Receptor Complexes on Rat Basophilic Leukemia Cells Does Not Change the Intrinsic Affinity but Can Alter the Kinetics of the Ligand-IgE Interaction†

Richard G. Posner,‡ Benjamin Lee,‡ Daniel H. Conrad,§ David Holowka,‡ Barbara Baird,‡ and Byron Goldstein*,‖
Department of Chemistry, Baker Laboratory, Cornell University, Ithaca, New York 14853, Department of Microbiology and Immunology, Medical College of Virginia, Box 678 MCV Station, Richmond, Virginia 23298, and Theoretical Biology and Biophysics Group, Theoretical Division, T-10, MS K710, Los Alamos National Laboratory, Los Alamos, New Mexico 87545
Received January 21, 1992

ABSTRACT: The aggregation of IgE anchored to high-affinity Fc_ϵ receptors on rat basophilic leukemia (RBL) cells by multivalent antigens initiates transmembrane signaling and ultimately cellular degranulation. Previous studies have shown that the rate of dissociation of bivalent and multivalent DNP ligands from RBL cells sensitized with anti-DNP IgE decreases with increasing ligand incubation times. One mechanism proposed for this effect is that when IgE molecules are aggregated, a conformational change occurs that results in an increase in the intrinsic affinity of IgE for antigen. This possibility was tested by measuring the equilibrium constant for the binding of monovalent DNP-lysine to anti-DNP IgE under two conditions, where the cell-bound IgE is dispersed and where it has been aggregated into visible patches on the cell surface using anti-IgE and a secondary antibody. No difference in the equilibrium constant in these two cases was observed. We also measured the rate of dissociation of a monovalent ligand from cell surface IgE under these two conditions. Whereas the affinity for monovalent ligand is not altered by IgE aggregation, we observe that the rate of ligand dissociation from IgE in clusters is slower than the rate of ligand dissociation from unaggregated IgE. These results are discussed in terms of recent theoretical developments concerning effects of receptor density on ligand binding to cell surfaces.

The cross-linking of immunoglobulin E (IgE)[1] bound to the high-affinity Fc_ϵ receptor ($Fc_\epsilon RI$) on the surface of mast cells, basophils, or their tumor analogue, rat basophilic leukemia (RBL) cells, is the first step in a cascade of events that culminates in cellular degranulation. In addition to initiating a variety of biochemical events, aggregation of IgE on RBL cells can be rapidly followed by internalization of IgE aggregates (Furuichi et al., 1984), increased fluid-phase pinocytosis, changes in the surface topology of the cell (Pfeiffer et al., 1985), an increase in the immobile fraction of cell surface IgE (Menon et al., 1986a; Myers et al., 1992), and interactions between Fc_ϵ receptors and the membrane skeleton (Robertson et al., 1986; Apgar, 1990).

Recently, fluorescence techniques to monitor the rate and extent of ligand binding to cell surface-bound IgE have been developed (Erickson et al., 1986, 1987, 1991; Seagrave et al., 1987). Seagrave et al. (1987) used flow cytometry to study the binding of a phycobilli protein highly conjugated with DNP groups (DNP_{42}-phycoerythrin) to RBL cells sensitized with anti-DNP IgE. They observed that this multivalent ligand became increasingly resistant to DNP-lysine-induced dissociation as the incubation time of the ligand with the cells was increased. With fluorescence quenching methods, we observed that a symmetric bivalent ligand with two DNP groups ($(DCT)_2Cys$) became increasingly resistant to dissociation induced by high concentrations of anti-DNP IgE in solution, but not by high concentrations of a monovalent hapten (DCT) (Erickson et al., 1991).

Two hypotheses have been proposed for the observed resistance of DNP_{42}-phycoerythrin to dissociation. In the first hypothesis, the aggregation of IgE-$Fc_\epsilon RI$ complexes triggers events that induce a conformational change in the IgE binding site resulting in an increase in its affinity for antigen (Seagrave et al., 1987). This type of change appears to occur with neutrophils which have receptors with both high and low affinity for the peptide ligand f-Met-Leu-Phe (Sklar et al., 1987). In this case, ligand binding induces a time-dependent conversion of the receptor from a low-affinity state to a high-affinity state that appears to be modulated by receptor interaction with a GTP-binding protein (Sklar et al., 1987). The second hypothesis is that a multivalent ligand binds to IgE-$Fc_\epsilon RI$ complexes which then form long-lived clusters associated with other cellular components (Seagrave et al., 1987; Erickson et al., 1991). Ligand dissociation from the cell surface is

† This work was supported by National Institutes of Health Grants GM35556, GM07273 and AI22449 and done under the auspices of the United States Department of Energy.
‡ Cornell University.
§ Medical College of Virginia.
‖ Los Alamos National Laboratory.

[1] IgE, immunoglobulin E; $Fc_\epsilon R1$, high-affinity Fc_ϵ receptor; RBL, rat basophilic leukemia; DNP, dinitrophenyl; DCT, [ε-[(2,4-dinitrophenyl)amino]caproyl]-L-tyrosine; FITC, fluorescein 5-isothiocyanate; $(DCT)_2Cys$, *N,N'*-bis[[ε-[(2,4-dinitrophenyl)amino]caproyl]-L-tyrosyl]-cystine; [^{3}H]-5HT, [1,2-^{3}H(N)]-5-hydroxytryptamine binoxalate.

0006-2960/92/0431-5350$03.00/0